EUROPEAN LABORATORY FOR PARTICLE PHYSICS

CERN-PPE/96-14
2 February 1996

Improved Measurement of the $\overline{B}^0$ and B^- Meson Lifetimes

The ALEPH Collaboration

Abstract

The lifetimes of the $\overline{B}^0$ and B^- mesons have been measured with the ALEPH detector at LEP, using approximately 3 million hadronic Z decays collected in the period 1991–1994. In the first of three methods, semileptonic decays of $\overline{B}^0$ and B^- mesons were partially reconstructed by identifying events containing a lepton with an associated D^{*+} or D^0 meson. The second method used fully reconstructed $\overline{B}^0$ and B^- mesons. The third method, used to measure the $\overline{B}^0$ lifetime, employed a partial reconstruction technique to identify $\overline{B}^0 \to D^{*+}\pi^- X$ decays.

The combined results are

$$\begin{aligned} \tau_0 &= 1.55 \pm 0.06 \pm 0.03 \text{ ps}, \\ \tau_- &= 1.58 \pm 0.09 \pm 0.03 \text{ ps}, \\ \frac{\tau_-}{\tau_0} &= 1.03 \pm 0.08 \pm 0.02. \end{aligned}$$

(Submitted to Zeitschrift für Physik C)

The ALEPH Collaboration

D. Buskulic, I. De Bonis, D. Decamp, P. Ghez, C. Goy, J.-P. Lees, A. Lucotte, M.-N. Minard, P. Odier, B. Pietrzyk

Laboratoire de Physique des Particules (LAPP), IN^{2}P^3-CNRS, 74019 Annecy-le-Vieux Cedex, France

M.P. Casado, M. Chmeissani, J.M. Crespo, M. Delfino,[12] I. Efthymiopoulos,[1] E. Fernandez, M. Fernandez-Bosman, Ll. Garrido,[15] A. Juste, M. Martinez, S. Orteu, A. Pacheco, C. Padilla, A. Pascual, J.A. Perlas, I. Riu, F. Sanchez, F. Teubert

Institut de Fisica d'Altes Energies, Universitat Autonoma de Barcelona, 08193 Bellaterra (Barcelona), Spain[7]

A. Colaleo, D. Creanza, M. de Palma, G. Gelao, M. Girone, G. Iaselli, G. Maggi,[3] M. Maggi, N. Marinelli, S. Nuzzo, A. Ranieri, G. Raso, F. Ruggieri, G. Selvaggi, L. Silvestris, P. Tempesta, G. Zito

Dipartimento di Fisica, INFN Sezione di Bari, 70126 Bari, Italy

X. Huang, J. Lin, Q. Ouyang, T. Wang, Y. Xie, R. Xu, S. Xue, J. Zhang, L. Zhang, W. Zhao

Institute of High-Energy Physics, Academia Sinica, Beijing, The People's Republic of China[8]

R. Alemany, A.O. Bazarko, G. Bonvicini,[23] M. Cattaneo, P. Comas, P. Coyle, H. Drevermann, R.W. Forty, M. Frank, R. Hagelberg, J. Harvey, P. Janot, B. Jost, E. Kneringer, J. Knobloch, I. Lehraus, E.B. Martin, P. Mato, A. Minten, R. Miquel, Ll.M. Mir,[2] L. Moneta, T. Oest,[20] F. Palla, J.R. Pater,[27] J.-F. Pusztaszeri, F. Ranjard, P. Rensing, L. Rolandi, D. Schlatter, M. Schmelling,[24] O. Schneider, W. Tejessy, I.R. Tomalin, A. Venturi, H. Wachsmuth, A. Wagner, T. Wildish

European Laboratory for Particle Physics (CERN), 1211 Geneva 23, Switzerland

Z. Ajaltouni, A. Barrès, C. Boyer, A. Falvard, P. Gay, C . Guicheney, P. Henrard, J. Jousset, B. Michel, S. Monteil, J-C. Montret, D. Pallin, P. Perret, F. Podlyski, J. Proriol, J.-M. Rossignol

Laboratoire de Physique Corpusculaire, Université Blaise Pascal, IN^{2}P^3-CNRS, Clermont-Ferrand, 63177 Aubière, France

T. Fearnley, J.B. Hansen, J.D. Hansen, J.R. Hansen, P.H. Hansen, B.S. Nilsson, A. Wäänänen

Niels Bohr Institute, 2100 Copenhagen, Denmark[9]

A. Kyriakis, C. Markou, E. Simopoulou, I. Siotis, A. Vayaki, K. Zachariadou

Nuclear Research Center Demokritos (NRCD), Athens, Greece

A. Blondel, G. Bonneaud, J.C. Brient, P. Bourdon, A. Rougé, M. Rumpf, A. Valassi,[6] M. Verderi, H. Videau[21]

Laboratoire de Physique Nucléaire et des Hautes Energies, Ecole Polytechnique, IN^{2}P^3-CNRS, 91128 Palaiseau Cedex, France

D.J. Candlin, M.I. Parsons

Department of Physics, University of Edinburgh, Edinburgh EH9 3JZ, United Kingdom[10]

E. Focardi,[21] G. Parrini

Dipartimento di Fisica, Università di Firenze, INFN Sezione di Firenze, 50125 Firenze, Italy

M. Corden, C. Georgiopoulos, D.E. Jaffe

Supercomputer Computations Research Institute, Florida State University, Tallahassee, FL 32306-4052, USA [13,14]

A. Antonelli, G. Bencivenni, G. Bologna,[4] F. Bossi, P. Campana, G. Capon, D. Casper, V. Chiarella, G. Felici, P. Laurelli, G. Mannocchi,[5] F. Murtas, G.P. Murtas, L. Passalacqua, M. Pepe-Altarelli

Laboratori Nazionali dell'INFN (LNF-INFN), 00044 Frascati, Italy

L. Curtis, S.J. Dorris, A.W. Halley, I.G. Knowles, J.G. Lynch, V. O'Shea, C. Raine, P. Reeves, J.M. Scarr, K. Smith, A.S. Thompson, F. Thomson, S. Thorn, R.M. Turnbull

Department of Physics and Astronomy, University of Glasgow, Glasgow G12 8QQ,United Kingdom[10]

U. Becker, C. Geweniger, G. Graefe, P. Hanke, G. Hansper, V. Hepp, E.E. Kluge, A. Putzer, B. Rensch, M. Schmidt, J. Sommer, H. Stenzel, K. Tittel, S. Werner, M. Wunsch

Institut für Hochenergiephysik, Universität Heidelberg, 69120 Heidelberg, Fed. Rep. of Germany[16]

D. Abbaneo, R. Beuselinck, D.M. Binnie, W. Cameron, P.J. Dornan, A. Moutoussi, J. Nash, J.K. Sedgbeer, A.M. Stacey, M.D. Williams

Department of Physics, Imperial College, London SW7 2BZ, United Kingdom[10]

G. Dissertori, P. Girtler, D. Kuhn, G. Rudolph

Institut für Experimentalphysik, Universität Innsbruck, 6020 Innsbruck, Austria[18]

A.P. Betteridge, C.K. Bowdery, P. Colrain, G. Crawford, A.J. Finch, F. Foster, G. Hughes, T. Sloan, M.I. Williams

Department of Physics, University of Lancaster, Lancaster LA1 4YB, United Kingdom[10]

A. Galla, A.M. Greene, K. Kleinknecht, G. Quast, B. Renk, E. Rohne, H.-G. Sander, P. van Gemmeren C. Zeitnitz

Institut für Physik, Universität Mainz, 55099 Mainz, Fed. Rep. of Germany[16]

J.J. Aubert,[21] A.M. Bencheikh, C. Benchouk, A. Bonissent,[21] G. Bujosa, D. Calvet, J. Carr, C. Diaconu, F. Etienne, N. Konstantinidis, P. Payre, D. Rousseau, M. Talby, A. Sadouki, M. Thulasidas, K. Trabelsi

Centre de Physique des Particules, Faculté des Sciences de Luminy, IN^{2}P^3-CNRS, 13288 Marseille, France

M. Aleppo, F. Ragusa[21]

Dipartimento di Fisica, Università di Milano e INFN Sezione di Milano, 20133 Milano, Italy

I. Abt, R. Assmann, C. Bauer, W. Blum, H. Dietl, F. Dydak,[21] G. Ganis, C. Gotzhein, K. Jakobs, H. Kroha, G. Lütjens, G. Lutz, W. Männer, H.-G. Moser, R. Richter, A. Rosado-Schlosser, S. Schael, R. Settles, H. Seywerd, R. St. Denis, W. Wiedenmann, G. Wolf

Max-Planck-Institut für Physik, Werner-Heisenberg-Institut, 80805 München, Fed. Rep. of Germany[16]

J. Boucrot, O. Callot, A. Cordier, M. Davier, L. Duflot, J.-F. Grivaz, Ph. Heusse, M. Jacquet, D.W. Kim,[19] F. Le Diberder, J. Lefrançois, A.-M. Lutz, I. Nikolic, H.J. Park,[19] I.C. Park,[19] M.-H. Schune, S. Simion, J.-J. Veillet, I. Videau

Laboratoire de l'Accélérateur Linéaire, Université de Paris-Sud, IN^{2}P^3-CNRS, 91405 Orsay Cedex, France

P. Azzurri, G. Bagliesi, G. Batignani, S. Bettarini, C. Bozzi, G. Calderini, M. Carpinelli, M.A. Ciocci, V. Ciulli, R. Dell'Orso, R. Fantechi, I. Ferrante, L. Foà,[1] F. Forti, A. Giassi, M.A. Giorgi, A. Gregorio, F. Ligabue, A. Lusiani, P.S. Marrocchesi, A. Messineo, G. Rizzo, G. Sanguinetti, A. Sciabà, P. Spagnolo, J. Steinberger, R. Tenchini, G. Tonelli,[26] C. Vannini, P.G. Verdini, J. Walsh

Dipartimento di Fisica dell'Università, INFN Sezione di Pisa, e Scuola Normale Superiore, 56010 Pisa, Italy

G.A. Blair, L.M. Bryant, F. Cerutti, J.T. Chambers, Y. Gao, M.G. Green, T. Medcalf, P. Perrodo, J.A. Strong, J.H. von Wimmersperg-Toeller

Department of Physics, Royal Holloway & Bedford New College, University of London, Surrey TW20 OEX, United Kingdom[10]

D.R. Botterill, R.W. Clifft, T.R. Edgecock, S. Haywood, P. Maley, P.R. Norton, J.C. Thompson, A.E. Wright

Particle Physics Dept., Rutherford Appleton Laboratory, Chilton, Didcot, Oxon OX11 OQX, United Kingdom[10]

B. Bloch-Devaux, P. Colas, S. Emery, W. Kozanecki, E. Lançon, M.C. Lemaire, E. Locci, B. Marx, P. Perez, J. Rander, J.-F. Renardy, A. Roussarie, J.-P. Schuller, J. Schwindling, A. Trabelsi, B. Vallage

CEA, DAPNIA/Service de Physique des Particules, CE-Saclay, 91191 Gif-sur-Yvette Cedex, France[17]

S.N. Black, J.H. Dann, R.P. Johnson, H.Y. Kim, A.M. Litke, M.A. McNeil, G. Taylor

Institute for Particle Physics, University of California at Santa Cruz, Santa Cruz, CA 95064, USA[22]

C.N. Booth, R. Boswell, C.A.J. Brew, S. Cartwright, F. Combley, A. Koksal, M. Letho, W.M. Newton, J. Reeve, L.F. Thompson

Department of Physics, University of Sheffield, Sheffield S3 7RH, United Kingdom[10]

A. Böhrer, S. Brandt, V. Büscher, G. Cowan, C. Grupen, G. Lutters, J. Minguet-Rodriguez, F. Rivera,[25] P. Saraiva, L. Smolik, F. Stephan,

Fachbereich Physik, Universität Siegen, 57068 Siegen, Fed. Rep. of Germany[16]

M. Apollonio, L. Bosisio, R. Della Marina, G. Giannini, B. Gobbo, G. Musolino,

Dipartimento di Fisica, Università di Trieste e INFN Sezione di Trieste, 34127 Trieste, Italy

J. Rothberg, S. Wasserbaech

Experimental Elementary Particle Physics, University of Washington, WA 98195 Seattle, U.S.A.

S.R. Armstrong, L. Bellantoni,[30] P. Elmer, Z. Feng,[31] D.P.S. Ferguson, Y.S. Gao,[32] S. González, J. Grahl, T.C. Greening, J.L. Harton,[28] O.J. Hayes, H. Hu, P.A. McNamara III, J.M. Nachtman, W. Orejudos, Y.B. Pan, Y. Saadi, M. Schmitt, I.J. Scott, V. Sharma,[29] A.M. Walsh,[33] Sau Lan Wu, X. Wu, J.M. Yamartino, M. Zheng, G. Zobernig

Department of Physics, University of Wisconsin, Madison, WI 53706, USA[11]

---

[1] Now at CERN, 1211 Geneva 23, Switzerland.
[2] Supported by Dirección General de Investigación Científica y Técnica, Spain.
[3] Now at Dipartimento di Fisica, Università di Lecce, 73100 Lecce, Italy.
[4] Also Istituto di Fisica Generale, Università di Torino, Torino, Italy.
[5] Also Istituto di Cosmo-Geofisica del C.N.R., Torino, Italy.
[6] Supported by the Commission of the European Communities, contract ERBCHBICT941234.
[7] Supported by CICYT, Spain.
[8] Supported by the National Science Foundation of China.
[9] Supported by the Danish Natural Science Research Council.
[10] Supported by the UK Particle Physics and Astronomy Research Council.
[11] Supported by the US Department of Energy, grant DE-FG0295-ER40896.
[12] Also at Supercomputations Research Institute, Florida State University, Tallahassee, U.S.A.
[13] Supported by the US Department of Energy, contract DE-FG05-92ER40742.
[14] Supported by the US Department of Energy, contract DE-FC05-85ER250000.
[15] Permanent address: Universitat de Barcelona, 08208 Barcelona, Spain.
[16] Supported by the Bundesministerium für Forschung und Technologie, Fed. Rep. of Germany.
[17] Supported by the Direction des Sciences de la Matière, C.E.A.
[18] Supported by Fonds zur Förderung der wissenschaftlichen Forschung, Austria.
[19] Permanent address: Kangnung National University, Kangnung, Korea.
[20] Now at DESY, Hamburg, Germany.
[21] Also at CERN, 1211 Geneva 23, Switzerland.
[22] Supported by the US Department of Energy, grant DE-FG03-92ER40689.
[23] Now at Wayne State University, Detroit, MI 48202, USA.
[24] Now at Max-Plank-Institüt für Kernphysik, Heidelberg, Germany.
[25] Partially supported by Colciencias, Colombia.
[26] Also at Istituto di Matematica e Fisica, Università di Sassari, Sassari, Italy.
[27] Now at Schuster Laboratory, University of Manchester, Manchester M13 9PL, UK.
[28] Now at Colorado State University, Fort Collins, CO 80523, USA.
[29] Now at University of California at San Diego, La Jolla, CA 92093, USA.
[30] Now at Fermi National Accelerator Laboratory, Batavia, IL 60510, USA.
[31] Now at The Johns Hopkins University, Baltimore, MD 21218, U.S.A.
[32] Now at Harvard University, Cambridge, MA 02138, U.S.A.
[33] Now at Rutgers University, Piscataway, NJ 08855-0849, U.S.A.

1 Introduction

Measurements of the individual b hadron lifetimes represent a quantitative test of the present understanding of b hadron decay dynamics, where non-spectator effects such as Pauli interference and W-exchange may lead to different lifetimes for the different b hadrons [1]. The individual lifetimes are also necessary inputs when determining other quantities of interest in heavy flavour physics, such as the B_S^0 mixing parameter x_S and the CKM matrix element $|V_{cb}|$. Measurement precision on the order of a few percent is required because the predicted differences among the B meson lifetimes are approximately 5%.

This paper reports measurements of the $\overline{B}^0$ and B^- lifetimes obtained using the ALEPH detector at LEP. Previous measurements of these lifetimes are reported in [2, 3]. Here, three different techniques, all based on the same general method, have been used, yielding the most precise measurements to date. The decay length of each B candidate was measured using the reconstructed interaction point and B decay vertex. These vertices are reconstructed in three dimensions with good precision. Then, the distributions of the individual proper times, calculated using the measured decay length, mass, and momentum of each candidate, were fitted to extract the mean lifetime of the sample. The three analyses differ in the method used to reconstruct the B decay vertex and momentum. Fig. 1 shows a generic decay[1] $\overline{B}^0 \to D^{*+}X^-$ followed by $D^{*+} \to D^0\pi_D^+$. To reconstruct

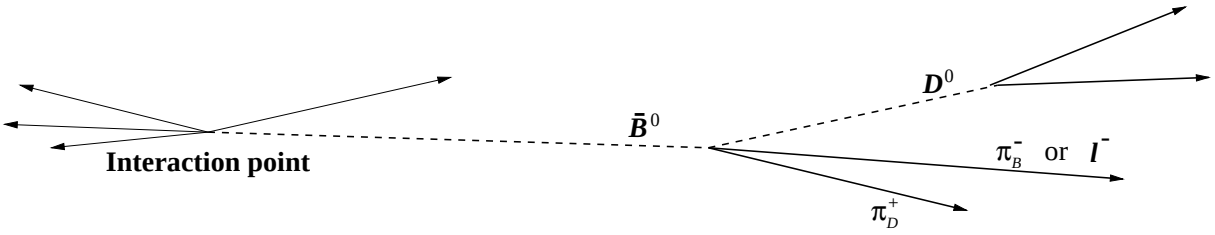

Figure 1: Schematic representation of B decay topologies reconstructed with the three methods described in this article.

such a candidate, the first analysis, which follows closely the method of [2], considered the semileptonic decay where X^- was $\ell^-\overline{\nu}$. With this technique, the D^0 candidate was fully reconstructed and combined with the pion candidate π_D^+ and the lepton candidate ℓ^- to identify the B meson candidate and determine its decay vertex. The B meson momentum was reconstructed using the charged track momenta and an estimate of the neutrino energy from the missing energy in the event. The second analysis used several fully reconstructed hadronic decay modes. An example of such a decay $\overline{B}^0 \to D^{*+}\pi_B^-$ is depicted in Fig. 1. Complete reconstruction of the B decay products allowed a direct determination of its decay vertex and momentum. The technique employed in the third analysis did not reconstruct the D^0 meson, but relied only on the two pions π_B^- and π_D^+ to identify the B candidate and to measure its momentum. The candidate decay length was measured by using these two pions and the jet direction.

[1] Charge conjugate modes are implied throughout this paper.

2 The ALEPH detector

The ALEPH detector is described in detail elsewhere [4]. A high resolution vertex detector (VDET) [5] consisting of two layers of silicon with double-sided readout provides precision tracking near the interaction region. It provides measurements in the $r\phi$ and z directions at average radii of 6.5 cm and 11.3 cm, with approximately 12 μm precision. The VDET provides full azimuthal coverage and polar angle coverage in the region $|\cos\theta| < 0.85$ for the inner layer only and $|\cos\theta| < 0.69$ for both layers. Outside the VDET particles traverse the inner tracking chamber (ITC) and the time projection chamber (TPC). The ITC is a cylindrical drift chamber with eight axial wire layers at radii between 16 and 26 cm. The TPC measures up to 21 space points per track at radii between 40 and 171 cm, and also provides up to 338 measurements of the specific energy loss ($\mathrm{d}E/\mathrm{d}x$) of each charged track. A K/π separation of approximately 2σ is achieved for charged tracks with momenta greater than 3 GeV/c. The quantity χ_H ($H = \pi$, K, etc.), used in the $\mathrm{d}E/\mathrm{d}x$ selection criteria, is defined as the difference between the measured and expected specific energy loss expressed in terms of standard deviations for the mass hypothesis H. Studies on simulated events have shown that the criterion $\chi_K + \chi_\pi < 1$ is more effective in selecting kaons and rejecting pions than a simple one-dimensional requirement on χ_K or χ_π. Tracking is performed in a 1.5 T magnetic field provided by a superconducting solenoid. The combined tracking system yields a momentum resolution of $\sigma(p_T)/p_T = 0.6 \times 10^{-3} p_T \oplus 0.005$ (p_T in GeV/c) and the impact parameter resolution is given by $\sigma(\delta) = 25 + 95/p$ μm (p in GeV/c) for both the $r\phi$ and z projections [6].

The electromagnetic calorimeter (ECAL) is a lead/wire-chamber sandwich operated in proportional mode. The calorimeter is read out in projective towers that subtend typically $0.9^\circ \times 0.9^\circ$ in solid angle and that are segmented in three longitudinal sections. The hadron calorimeter (HCAL) uses the iron return yoke as the absorber. Hadronic showers are sampled by 23 planes of streamer tubes, with analog projective tower and digital hit pattern readout. The HCAL is used in combination with two layers of muon chambers outside the magnet for muon identification.

The data samples used correspond to approximately 3 million hadronic decays of the Z boson, collected in the period 1991–1994. The charged track selection, common to all three analyses, required tracks to intersect an imaginary cylinder of radius 2 cm and half-length 4 cm centered on the nominal interaction point, have at least four TPC coordinates, have polar angles θ such that $|\cos\theta| < 0.95$ and have momenta greater than 200 MeV/c.

3 Measurements using $D^{(*)}\ell$ combinations

The method based on $D^{(*)}\ell$ combinations is able to measure separately the B^- and $\overline{B}^0$ lifetimes by exploiting the fact that B^- and $\overline{B}^0$ mesons can be selected with purities between 70% and 80% by identifying events containing a D^0-lepton pair ($D^0\ell^-$) or D^{*+}-lepton pair ($D^{*+}\ell^-$), respectively.

3.1 Candidate selection

The $D^{*+}\ell^-$ and $D^0\ell^-$ event samples consist of an identified lepton (e or μ) associated with a D^{*+} or D^0 candidate. The selection of muons and electrons is described in detail in ref. [7]. For this analysis, lepton candidates were required to have momenta of at least 3 GeV/c. D^{*+} and D^0 candidates were reconstructed from charged tracks that formed an angle of less than 45° with the lepton candidate.

The D^{*+} candidates were identified via the decay $D^{*+} \to D^0\pi^+$, followed by either $D^0 \to K^-\pi^+$, $D^0 \to K^-\pi^+\pi^-\pi^+$ or $D^0 \to K^-\pi^+\pi^0$. The difference in mass between the D^{*+} and D^0 candidates was required to lie within 1.5 MeV/c^2 (approximately two standard deviations of the experimental resolution) of the world average value of 145.6 MeV/c^2 [8].

The three $D^{*+}\ell^-$ subsamples suffer from varying amounts of background, so different selection criteria have been chosen for each channel. For the subsample where $D^0 \to K^-\pi^+$, the momentum of the D^0 was required to be greater than 5 GeV/c.

The other two $D^{*+}\ell^-$ subsamples suffer from greater combinatorial background and therefore more stringent selection criteria were applied. For the $D^0 \to K^-\pi^+\pi^-\pi^+$ channel, the D^0 momentum had to be greater than 8 GeV/c. When dE/dx information was available for the K track (at least 50 wire measurements), it was required to satisfy $\chi_K + \chi_\pi < 1$ (Sect. 2). At least two of the D^0 decay tracks had to have momentum greater than 1 GeV/c. If, for a given detected lepton, more than one combination satisfied these selection criteria, the best combination was selected, based on the value of the χ^2 of the B vertex fit (discussed below).

For the $D^0 \to K^-\pi^+\pi^0$ channel, π^0's were reconstructed from pairs of photons identified in ECAL. The momenta of the π^0 candidates were corrected by performing a fit which constrained the candidate mass to the π^0 mass. Neutral pion candidates with momenta greater than 2 GeV/c were used to form D^0 candidates. The momenta of the D^0 candidates were required to be greater than 10 GeV/c, while the two charged tracks in the decay were required to have at least 0.5 GeV/c of momentum. The same dE/dx criterion was applied to this channel as to the $D^0 \to K^-\pi^+\pi^-\pi^+$ channel above. Furthermore the decay kinematics were required to be consistent with at least one of three possible resonant final states, which nearly saturate the total $K^-\pi^+\pi^0$ rate: $K^-\rho^+$, $K^{*-}\pi^+$ or $\overline{K}^{*0}\pi^0$. For each decay hypothesis the mass of the resonant particle and the cosine of the helicity angle, defined as the angle between the scalar particle and one of the decay products of the vector particle calculated in the rest frame of the vector particle, were calculated. The helicity angle is distributed as $\cos^2\theta_H$ for the resonant states listed above. If the mass was within two standard deviations of the expected value (both the natural widths of the resonances and the mass resolution were taken into account) and the absolute value of the cosine of the helicity angle was greater than 0.4, the candidate was considered consistent with the resonant decay hypothesis. In the case of more than one D^0 candidate per identified lepton, the candidate with the measured value of $M_{D^0\pi} - M_{D^0}$ that is closest to the expected mass difference was chosen. For this channel it was not possible to use the B vertex χ^2 criterion, as in the $D^0 \to K^-\pi^+\pi^-\pi^+$ case, because here multiple D^0 candidates arise from more than one π^0 candidate with the same charged track pair. The B vertex fit χ^2 is nearly identical for such multiple candidates since it depends almost entirely on the two charged tracks.

Table 1: Fitted D^0 mass and width and number of D^0 candidates and combinatorial background events falling within two standard deviations of the fitted mass. The uncertainties are statistical only.

Subsample		Mass (MeV/c^2)	Width (MeV/c^2)	Signal Events	Background Events
$D^{*+}\ell^-$	$D^0 \to K^-\pi^+$	1863.7 ± 0.7	7.9 ± 0.6	324 ± 19	27 ± 6
	$D^0 \to K^-\pi^+\pi^-\pi^+$	1862.6 ± 0.7	6.5 ± 0.7	290 ± 18	37 ± 7
	$D^0 \to K^-\pi^+\pi^0$	1862.4 ± 2.7	32.3 ± 2.5	251 ± 17	38 ± 11
$D^0\ell^-$	$D^0 \to K^-\pi^+$	1863.6 ± 0.5	8.7 ± 0.5	672 ± 29	111 ± 26

The $D^0\ell^-$ sample consists of events with a lepton and a D^0 candidate, where the D^0 was not the decay product of a D^{*+}. D^0 candidates were identified via the decay $D^0 \to K^-\pi^+$. For this sample, the powerful selection criterion involving the D^{*+}-D^0 mass difference was not applicable, making it necessary to apply stricter D^0 selection criteria. The D^0 candidates were required to have D^0, kaon and pion candidate momenta greater than 8 GeV/c, 2 GeV/c and 1.5 GeV/c, respectively. Furthermore, both tracks were required to have specific ionization compatible with the particular particle hypothesis. To reject D^0 candidates coming from $D^{*+} \to D^0\pi^+$, a search for the additional pion was performed. If a pion candidate yielding a D^{*+}-D^0 mass difference within 1.5 MeV/c^2 of the expected value was found, the $D^0\ell^-$ candidate was rejected. The efficiency for reconstructing the additional pion and rejecting D^0's coming from D^{*+} decays was found to be 84 ± 3 %.

To improve the signal to background ratio and to ensure well-measured decay lengths, additional selection criteria were placed on all the subsamples. The invariant mass of the $D^{(*)}\ell$ (where $D^{(*)}$ can be D^{*+} or D^0) system was required to be greater than 3 GeV/c^2. To exploit the high precision of the silicon vertex detector, the lepton track and at least two of the D^0 decay product tracks were required to have at least one VDET hit in both the $r\phi$ and z projections. Also, the D and B decay vertices were reconstructed (as will be discussed in Sect. 3.2) and the χ^2 probability for each vertex fit was required to be greater than 1%.

The D^0 candidate mass spectra for the four subsamples are shown in Fig. 2. The fitted curves consist of a Gaussian for the signal plus a linear background. The fitted D^0 mass and the fitted number of signal and background events within a window of $\pm 2\sigma$, where σ is the fitted width, around the fitted mass for the four subsamples are shown in Table 1.

3.2 B proper time reconstruction

Events reconstructed with a D^0 mass within two standard deviations of the fitted D^0 mass were selected for the lifetime analysis, resulting in 948 $D^{*+}\ell^-$ and 778 $D^0\ell^-$ candidates. One event was removed from the $D^{*+}\ell^-$ sample because it was also selected in the hadronic decay analysis (Sect. 4). The proper time t was obtained from the measured decay length and B momentum and the nominal B mass.

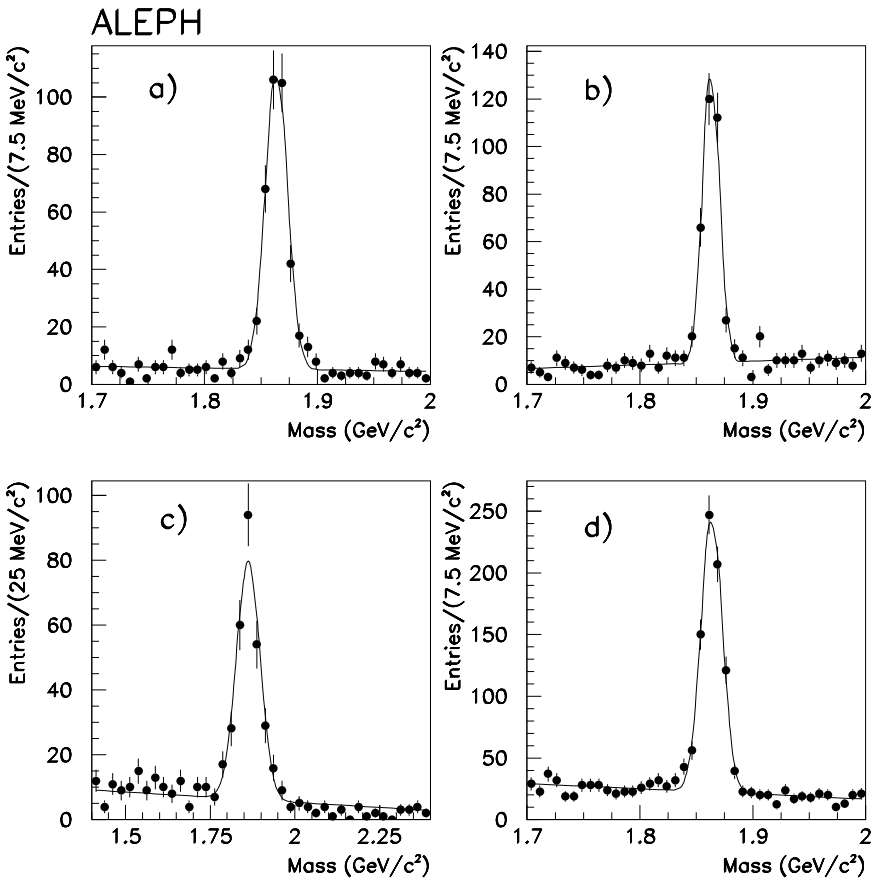

Figure 2: The invariant mass of D^0 candidates for the four subsamples: a) $D^{*+}\ell^-$, $D^0 \to K\pi$, b) $D^{*+}\ell^-$, $D^0 \to K\pi\pi\pi$, c) $D^{*+}\ell^-$, $D^0 \to K\pi\pi^0$, d) $D^0\ell^-$, $D^0 \to K\pi$. The smooth curves are results of the fit described in the text.

The decay length has been calculated by reconstructing the primary and B decay vertices in three dimensions. The primary vertex reconstruction algorithm [9], applied to simulated $b\overline{b}$ events, yields an average resolution of 50μm $\times$ 10μm $\times$ 60μm (horizontal $\times$ vertical $\times$ beam direction). The B decay vertex was obtained by first reconstructing the D^0 decay vertex using its known decay tracks and then extrapolating the neutral D^0 track backwards where it was combined with the lepton to form the B decay vertex. For the $D^0 \to K^-\pi^+\pi^0$ channel, the D^0 vertex was constructed using only the charged tracks, but the π^0 momentum was included when extrapolating the neutral D^0 track backwards to form the B vertex. In the case of $D^{*+}\ell^-$ events, the soft pion from the D^{*+} decay does not improve the resolution on the B decay length and was therefore not used in the reconstruction of the B vertex.

An estimate of the B decay length was obtained by projecting the distance between the primary and B decay vertices onto the direction defined by the $D^{(*)}\ell$ system. The uncertainty on the flight direction due to the missing neutrino induces a negligible error on the decay length. The resolution on the B decay length is typically 300 μm, compared with an average B decay length of approximately 2.5 mm. Monte Carlo studies showed

that the distribution of the decay length divided by its error (calcuated for each candidate) is well parametrized by the sum of two Gaussian functions. The values of the parameters that define this resolution function, the two widths and the fractional area of the wider Gaussian, were found to be 1.10 ± 0.07, 2.76 ± 0.35 and 0.16 ± 0.05, respectively, where the uncertainties are statistical.

The B momentum is reconstructed using an energy flow technique as described in [10]. The momentum resolution obtained using this technique depends on the selection criteria and varies between 10% and 15%, depending on the decay channel.

3.3 $\overline{B}^0$ and B^- lifetime measurement

Both the $D^{*+}\ell^-$ and $D^0\ell^-$ samples contain a mixture of $\overline{B}^0$ and B^- decays and the $B^-/\overline{B}^0$ mixture in the samples depends on the ratio of the lifetimes, as will be discussed below. Therefore, to measure the $\overline{B}^0$ and B^- lifetimes a simultaneous unbinned maximum likelihood fit to all the events was performed. The likelihood function contains three components for each sample and is written as

$$\begin{aligned}\mathcal{L} &= \prod_{i=1}^{N_{D^*\ell}} \left[f_-^* \mathcal{P}(t_i, \sigma_i, \tau_-) + f_0^* \mathcal{P}(t_i, \sigma_i, \tau_0) + f_{\rm BG}^* \mathcal{P}_{\rm BG}^*(t_i) \right] \\ &\times \prod_{i=1}^{N_{D^0\ell}} \left[f_-^0 \mathcal{P}(t_i, \sigma_i, \tau_-) + f_0^0 \mathcal{P}(t_i, \sigma_i, \tau_0) + f_{\rm BG}^0 \mathcal{P}_{\rm BG}^0(t_i) \right], \end{aligned} \quad (1)$$

where $\mathcal{P}(t, \sigma, \tau)$ is the probability function for the signal, consisting of an exponential function convolved with momentum and decay length resolution functions. The coefficients f_-^* and f_0^* are the fractions of the $D^{*+}\ell^-$ sample arising from B^- and $\overline{B}^0$ decays, respectively. Similarly, f_-^0 and f_0^0 are the fractions of the $D^0\ell^-$ sample coming from B^- and $\overline{B}^0$ decays. The coefficients $f_{\rm BG}^*$ and $f_{\rm BG}^0$ are the background fractions of the samples, while the functions $\mathcal{P}_{\rm BG}^*(t)$ and $\mathcal{P}_{\rm BG}^0(t)$ are the normalised proper time distributions of the background.

3.3.1 Signal composition

The composition of the signal (specified by the coefficients f_-^*, f_0^*, f_-^0 and f_0^0 of Eq. 1) must be calculated to complete the specification of the likelihood function. The difficulty in evaluating the signal composition arises from incomplete knowledge of the branching ratios of certain decay modes that contribute to the two samples.

The $\overline{B}^0$ and B^- content of the two samples were calculated as follows. The relevant semileptonic branching ratios for $\overline{B}^0$ mesons were taken from measurements at the $\Upsilon(4S)$ energy. Where measurements were incomplete, isospin conservation was applied, as well as the constraint that the sum of the exclusive channels equals the inclusive $\overline{B}^0$ semileptonic branching ratio. The B^- branching fractions were then obtained from

$$B(B^- \to \ell^- X) = \frac{\tau_-}{\tau_0} B(\overline{B}^0 \to \ell^- X'), \quad (2)$$

which derives from the expectation that the partial semileptonic decay widths are equal. The sample coefficients were then calculated by considering the $\overline{B}^0$ and B^- decay channels

that contribute to the $D^{*+}\ell^-$ and $D^0\ell^-$ samples. As a consequence of this procedure, the coefficients f_-^*, f_0^*, f_-^0 and f_0^0 appearing in the likelihood function (Eq. 1) depend on the lifetime ratio. The full calculation, reported in the Appendix, shows that, for equal lifetimes, $87\pm4\%$ of the B decays in the $D^{*+}\ell^-$ sample are attributed to $\overline{B}^0$, while $75\pm5\%$ of the $D^0\ell^-$ sample B decays come from B^-.

3.3.2 Backgrounds

Background contamination arises from the following sources:

(1) combinatorial background, i.e. candidates with a misidentified $D^{(*)}$;

(2) the processes $\overline{B} \to D_s^- D^{(*)} X$, followed by $D_s^- \to \ell^- X$; and $\overline{B} \to D^{(*)}\tau^-\bar{\nu}X$, followed by $\tau^- \to \ell^-\nu\bar{\nu}$, give rise to a real $D^{(*)}$ and a real lepton;

(3) a real $D^{(*)}$ meson accompanied by a misidentified hadron (fake lepton) or non-prompt lepton, from $Z \to b\bar{b}$ or $Z \to c\bar{c}$ events.

Source (1) is the dominant background and its contribution is determined from a fit to the D^0 mass distributions. Its magnitude is given in Table 1 for the various subsamples. The proper time distribution for this source has been determined from the data by selecting events from the upper sideband of the D^0 peak. The same selection criteria described in Sect. 3.1 have been applied to the background samples, except that the requirement on the D^{*+}–D^0 mass difference in the case of the $D^{*+}\ell^-$ events has been removed to increase the statistics. A function consisting of a Gaussian plus two positive and two negative exponential tails was used to describe the temporal behaviour of these data.

The contribution from source (2) was calculated from the measured branching ratios for these process [8, 11, 12] plus a Monte Carlo simulation to determine the detection efficiency. This background accounts for 3–4% of the samples, depending on the channel.

The background from source (3) was estimated by considering wrong-sign ($D^{*+}\ell^+$ or $D^0\ell^+$) combinations and was found to contribute $3.0 \pm 1.5\%$ to the samples. Simulated events were used to determine the proper time distribution for sources (2) and (3).

3.3.3 Fit results

An unbinned maximum likelihood fit to the proper time distributions of the $D^{*+}\ell^-$ and $D^0\ell^-$ events was performed to determine the two free parameters τ_0 and τ_-. The values obtained are

$$\begin{aligned} \tau_0 &= 1.61 \pm 0.07 \text{ ps}, \\ \tau_- &= 1.58 \pm 0.09 \text{ ps}, \end{aligned}$$

where the uncertainties are statistical only. The correlation coefficient is -0.35. The ratio of the lifetimes is

$$\frac{\tau_-}{\tau_0} = 0.98 \pm 0.08,$$

taking into account the correlation between the lifetimes.

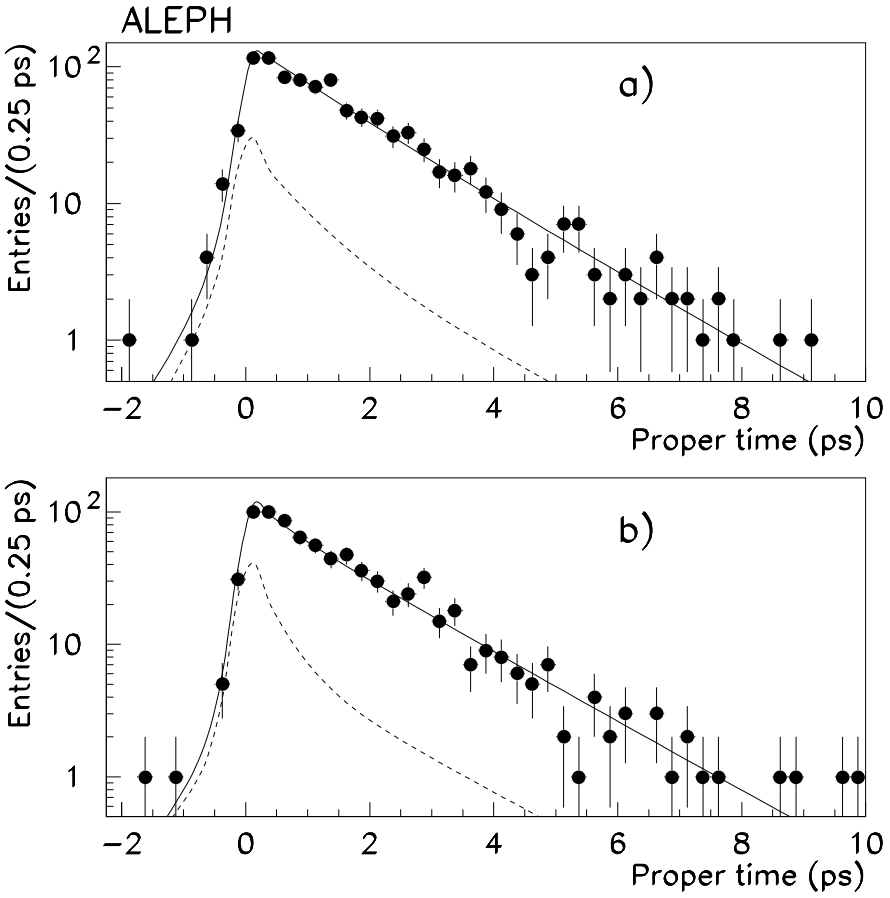

Figure 3: Proper time distributions with result of the fit overlaid for the two samples. a) $D^{*+}\ell^-$ events; b) $D^0\ell^-$ events; the dashed curves represent the background contribution to the fit, and the solid curves show the total fit. Not shown on the plots are a total of three candidates with measured proper times greater than 10 ps.

The proper time distributions of the two samples are shown in Fig. 3, with the results of the fit overlaid.

As a check on the procedure, a measurement of the D^0 lifetime has been performed. The D^0 flight distance is calculated as the distance between the B and D^0 decay vertices, projected onto the D^0 direction. An unbinned likelihood fit to the 1727 events yields

$$\tau_{D^0} = 0.404 \pm 0.012 \text{ (stat) ps},$$

in agreement with the world average value $\tau_{D^0} = 0.415 \pm 0.004$ ps [8].

3.3.4 Systematic uncertainties

Several sources of systematic uncertainty have been considered and are summarized in Table 2.

The systematic uncertainty in the B momentum resolution comes mainly from the uncertainty in the D^{**} content of semileptonic B decays. There is approximately a 2%

Table 2: Systematic uncertainties on the fitted lifetimes from the $D^{(*)}\ell$ analysis.

Source of uncertainty	τ_0 (ps)	τ_- (ps)	τ_-/τ_0
B momentum reconstruction	$^{+0.030}_{-0.027}$	$^{+0.030}_{-0.027}$	± 0.010
Background treatment	± 0.025	± 0.023	± 0.014
Signal composition	± 0.013	± 0.018	± 0.015
Decay length resolution	± 0.010	± 0.010	± 0.010
$D^{(*)}\pi\ell^-\nu$ relative efficiency	± 0.008	± 0.007	± 0.008
Total	$^{+0.043}_{-0.041}$	$^{+0.044}_{-0.042}$	± 0.026

uncertainty on the B momentum resolution function [10].

Uncertainties in the background fractions and proper time distributions have been considered. Different background samples have been selected by varying the sideband regions (for example, adding events from the lower sideband, which were excluded when determining the lifetime) and by using events with wrong-sign correlations. Additionally, an alternative parametrization of the proper time distributions (Gaussian plus one positive and one negative exponential tail) was tried and the resulting differences in the fitted lifetimes were taken as a systematic uncertainty.

The systematic uncertainty due to the signal composition was determined by varying the independent branching fractions within their uncertainties (Appendix). In principle, the fitted number of $D^{*+}\ell^-$ candidates could be overestimated due to the possible presence of a real D^0 combined with a random track such that the value of $M_{D^0\pi} - M_{D^0}$ falls within the signal region. The level of such an effect was found to be less than 1% by considering the sidebands of the $M_{D^0\pi} - M_{D^0}$ distribution. The uncertainty on the lifetime measurement due to this effect is included.

Although the signal composition coefficients are independent of the nominal reconstruction efficiencies, the relative efficiencies

$$\epsilon^{**} = \frac{\epsilon(B \to D^{(*)}\pi\ell\nu)}{\epsilon(B \to D^{(*)}\ell\nu)}$$

enter into the calculation and this uncertainty has been propagated to the systematic uncertainty on the lifetimes. The values of ϵ^{**} and their uncertainties are given in the Appendix.

The uncertainty due to the decay length resolution function was estimated by allowing a variation of its parameters consistent with their statistical error plus a systematic effect due to uncertainties in the Monte Carlo model of the decay length resolution.

4 Measurements using fully reconstructed hadronic decays

In the second method, the B^- and $\overline{B}^0$ candidates were fully reconstructed using some of their hadronic decay modes $B \to DX$ and $B \to \psi X$ (Table 3). This method leads to the reconstruction of the B decay length with a resolution of about 200 μm and of the B boost with a resolution better than 1%. The resolution on the boost is better than that obtained on the momentum due to correlations between the reconstructed mass and momentum of the B candidate. Moreover, the B^- and $\overline{B}^0$ samples are very well separated. Nevertheless, the number of candidates which can be reconstructed with such a method is small, due to the small branching fractions of hadronic decays and to their low selection efficiency.

Table 3: List of B decay channels and their sub-channels with the number of candidates (D^{*+} decays to $D^0\pi^+$).

$B \longrightarrow DX$	$D^0 \longrightarrow$				$D^+ \longrightarrow$
decay channels	$K^-\pi^+$	$K^-\pi^+\pi^0$	$K^-\pi^+\pi^+\pi^-$	$K^0_S\pi^+\pi^-$	$K^-\pi^+\pi^+$
$B^- \to D^0\pi^-$	16	13	35	1	
$B^- \to D^0 a_1^-(\to \pi^+\pi^-\pi^-)$	8			3	
$\overline{B}^0 \to D^+\pi^-$					29
$\overline{B}^0 \to D^{*+}\pi^-$	14	13	19	2	
$\overline{B}^0 \to D^{*+}\rho^-(\to \pi^-\pi^0)$	0		10	2	
$\overline{B}^0 \to D^{*+}a_1^-(\to \pi^+\pi^-\pi^-)$	8	8		2	

$B \longrightarrow \psi X$	$J/\psi \longrightarrow$	$\psi(2S) \longrightarrow$	
decay channels	e^+e^-, $\mu^+\mu^-$	e^+e^-, $\mu^+\mu^-$	$J/\psi\pi^+\pi^-$
$B^- \to \psi K^-$	13	3	1
$B^- \to \psi K^{*-}(\to K^0_S\pi^-)$	1	0	
$\overline{B}^0 \to \psi K^0_S$	3	1	0
$\overline{B}^0 \to \psi \overline{K}^{*0}(\to K^-\pi^+)$	10	0	

4.1 Candidate selection

Electrons and muons with momenta greater than 1 GeV/c and 2.5 GeV/c, respectively, were selected for this analysis. Charged kaon candidates were required to have momenta greater than 2 GeV/c and specific energy loss such that $\chi_K > -2.5$ and $\chi_K + \chi_\pi < 1$. For charged pion candidates $|\chi_\pi| < 3$ was required. Neutral kaons were reconstructed in the decay mode $K^0_S \to \pi^+\pi^-$.

Table 4: Mass windows used for the D candidates, minimum values of p_D, p_X and X_B required (or range of values when different criteria were applied for different sub-channels), and backgrounds rejected in the $B \to DX$ channels selection.

B decay	$m - m_D$ (MeV/c^2)	p_D (GeV/c)	p_X (GeV/c)	X_B	Rejection
$B^- \to D^0 X^-$	$\pm 15 \to \pm 30$	$4 \to 9$	6	0.7	D^0 from D^{*+}
$\overline{B}^0 \to D^+ \pi^-$	± 25	8	6	0.65	D_s^+, Λ_c^+
$\overline{B}^0 \to D^{*+} X^-$	± 30	4	$5 \to 9$	0.5	

To reconstruct the $B \to DX$ channels, cuts were applied on the D candidate momentum (p_D), the X particle momentum (p_X) and the B candidate energy ($X_B = E_B/E_{\rm beam}$), as shown in Table 4. With the exception of the $K^-\pi^+$ channel, the D^0 final states were required to be consistent with the presence of a vector meson (ρ or K^*). In particular, the $D^0 \to K^0_S \pi^+\pi^-$ candidates had to be consistent with either $K^{*-}\pi^+$ or $K^{*+}\pi^-$. This requirement was necessary to distinguish between D^0 and $\overline{D}^0$. The difference in mass between the D^{*+} and D^0 candidate was required to be within 2 MeV/c^2 of the expected value. Cuts were also applied on $\cos\theta^*$ (θ^* is the angle between the D and B meson flight directions in the B rest frame) for two channels: $-0.7 < \cos\theta^* < 0.4$ for $B^- \to D^0 a_1^-$ and $\cos\theta^* > -0.5$ for $\overline{B}^0 \to D^+\pi^-$. Care was taken to reduce possible contamination from other b hadrons. In particular, particle misidentification can lead to D_s^+ or Λ_c^+ being identified as a D^+. Therefore, D^+ candidates consistent with D_s^+ or Λ_c^+, under appropriate particle mass assignments, were rejected. The mass windows used to select the ψ candidates were ± 100 MeV/c^2 for ψ decaying directly to two leptons and ± 200 MeV/c^2 for $\psi(2S) \to J/\psi\pi^+\pi^-$. For this last channel the $\pi^+\pi^-$ mass was required to be greater than 0.4 GeV/c^2.

At least two tracks with vertex detector hits in both the $r\phi$ and z views were required for the D and ψX vertices. For the $B \to DX$ decay vertex, one additional track from the X candidate had to have vertex detector hits. Each secondary vertex was required to have a probability greater than 0.5%. In events with more than one B candidate in a mass window of $\pm$ 1 GeV/c^2 around the nominal B mass, only the candidate with the best vertex probability was retained.

4.2 B^- and $\overline{B}^0$ signal

The mass spectra of the candidates obtained after all selection cuts are shown in Fig. 4. A total of 94 B^- and 121 $\overline{B}^0$ candidates were selected, within a mass window of ± 60 MeV/c^2 around the B meson mass.

A fraction of the signal events ($11.3 \pm 2.1\%$) were mis-reconstructed using particles from fragmentation. These candidates have correct decay lengths but degraded measurement of the boost, the boost resolution being about 1% for half of them and around 20% for the remaining half. These mis-reconstructed candidates can be separated into two components. The first component (called corrupted signal) occurs when a soft pion

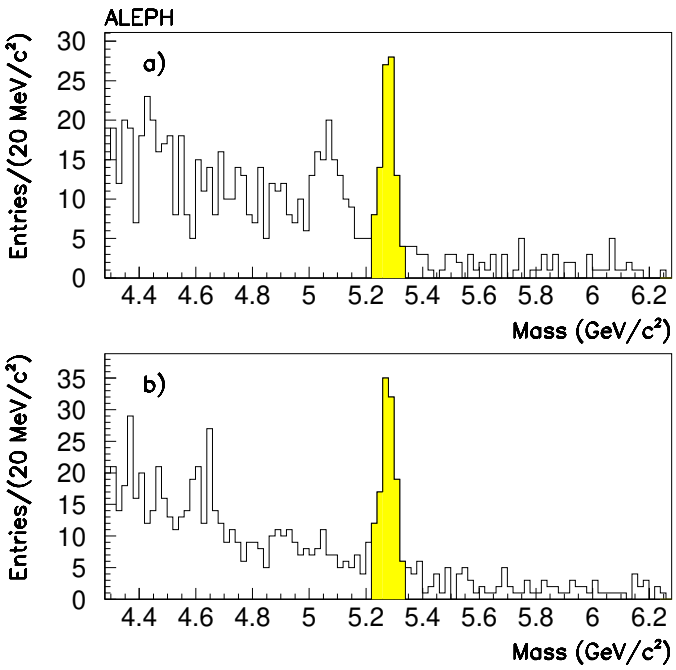

Figure 4: a) Mass spectrum of the reconstructed B^- candidates; b) the mass spectrum for the $\overline{B}^0$ candidates. Selected candidates are shaded. The peak near 5.1 GeV/c^2 in the B^- mass spectrum is due mainly to $B^- \to D^{*0}(\to D^0\pi^0)X^-$ and secondarily to $\overline{B}^0 \to D^{*+}(\to D^0\pi^+)X^-$, when the soft pion is not identified.

from the B decay products goes undetected or when a low momentum neutral or charged particle from fragmentation is included among the B candidate decay products. The efficiency for this component does not depend on proper time. The proper time distribution of such candidates found in a $b\overline{b}$ simulation was fitted with an exponential, yielding a lifetime in good agreement with the generated lifetime and so these candidates were taken as signal in the final fit. The second component (called physical background) contains candidates which were reconstructed using one high momentum or a few charged particles from fragmentation. These candidates can only be reconstructed if their decay length is very short, allowing charged particles from the primary vertex to be associated with their decay vertex, leading to a selection efficiency which decreases quickly at high decay length. The proper time distribution of these candidates found in a $b\overline{b}$ simulation has been fitted, yielding a lifetime of $\tau_{\rm phys} = 0.31^{+0.13}_{-0.09}$ ps for this sample which represents $f_{\tau_{\rm phys}} = 3.4\%$ of the B^- signal sample and $f_{\tau_{\rm phys}} = 5.6\%$ of the $\overline{B}^0$ signal sample. Separate fits of $\tau_{\rm phys}$ to the distributions of B^- and $\overline{B}^0$ samples give results in good agreement. This small low-lifetime component was taken into account in the final fit. The selected samples also contain a small contamination from other b hadrons which represents about 2% of the signal. This contamination was taken into account when evaluating the systematic uncertainties. Finally, the samples selected contain combinatorial background candidates originating from non-$b\overline{b}$ events with zero lifetime and a small component of combinatorial background events with non-zero lifetime from $c\overline{c}$ events and $b\overline{b}$ events.

4.3 $\overline{B}^0$ and B^- lifetime measurements

The position of the B decay vertex was reconstructed in three dimensions. The decay length was obtained by projecting the vector joining the interaction point and the B decay vertex onto the B momentum vector. The proper time t of each candidate was calculated from the reconstructed decay length, mass and momentum. The uncertainty on the proper time was calculated for each candidate using the uncertainty on the reconstructed decay length calculated event by event.

The proper time distribution of the combinatorial background was studied on the data using three background samples. For the $B \to DX$ channels, the wrong sign candidates were selected as, for example, $D^{*+}X^+$, $D^+\pi^+$ or D^0X^+. For the $B \to \psi X$ channels, wrong sign candidates were selected using "ψ"$\to \ell^\pm\ell^\pm$. The second background sample, containing the sideband candidates, was constructed using fake D or ψ candidates extracted from their mass spectrum sidebands. The "wrong sign sideband" candidates, constructed combining the previous two techniques, comprised the third background sample. Candidates for all background samples were required to have a mass the B sideband region, 5.4 GeV/c^2 to 6.3 GeV/c^2.

The calculated uncertainty on the decay length was checked on the background sample (removing the B sideband requirement to increase the statistics) by fitting the distribution of decay length divided by its uncertainty with a function comprised of a Gaussian and an exponential. The width of the Gaussian part was found to be $S = 1.27 \pm 0.03$, instead of unity, as would be expected if the decay length uncertainty were accurately estimated. Therefore, the calculated decay length uncertainty of each candidate was corrected by multiplying by the factor S.

The fraction of combinatorial background with non-zero lifetime ($f^{\psi,D}_{\tau_{\rm comb}}$) and its lifetime ($\tau_{\rm comb}$) were measured in the data using these three background samples, separately for the $B \to DX$ and $B \to \psi X$ channels. The proper time distribution of the $B \to \psi X$ background candidates from the three background samples plus events satisfying the standard selection but falling above the B mass region was fitted with a Gaussian centered at zero plus an exponential convolved with a Gaussian; the result of this fit is $f^{\psi}_{\tau_{\rm comb}} = 50 \pm 11\%$ and $\tau_{\rm comb} = 0.72 \pm 0.03$ ps. The proper time distribution of the $B \to DX$ background candidates from the three background samples was fitted with the previous background proper time function. Using the value for $\tau_{\rm comb}$ from $B \to \psi X$ channels, the result of the fit is $f^{D}_{\tau_{\rm comb}} = 3.9 \pm 1.5\%$. Since this non-zero lifetime fraction is so small, a fit with both $\tau_{\rm comb}$ and $f^{D}_{\tau_{\rm comb}}$ free does not converge in this channel, and thus the same value of $\tau_{\rm comb}$ was used for both channels.

The proper time distributions of the B^- and $\overline{B}^0$ samples were fitted separately by maximizing a likelihood function simultaneously on the $B \to DX$ and $B \to \psi X$ samples, with two different signal fractions $f^D_{\rm sig}$ and $f^{\psi}_{\rm sig}$:

$$\mathcal{L}(\tau_B, f^D_{\rm sig}, f^{\psi}_{\rm sig}) = \prod_{B\to DX} \mathcal{P}(t, \sigma_t, \tau_B, f^D_{\rm sig}) \times \prod_{B\to \psi X} \mathcal{P}(t, \sigma_t, \tau_B, f^{\psi}_{\rm sig}),$$

with $\mathcal{P}(t, \sigma_t, \tau_B, f_{\rm sig}) = f_{\rm sig}\mathcal{P}_{\rm sig}(t, \sigma_t, \tau_B) + f_{\rm phys}\mathcal{P}_{\rm phys}(t, \sigma_t) + f_{\rm comb}\mathcal{P}_{\rm comb}(t, \sigma_t)$. The signal proper time distribution $\mathcal{P}_{\rm sig}$ was an exponential convolved with a Gaussian. The physical background function $\mathcal{P}_{\rm phys}$ was an exponential with a lifetime of $\tau_{\rm phys}$ convolved with a Gaussian and its fraction was defined as $f_{\rm phys} = \frac{f_{\rm sig} f_{\tau_{\rm phys}}}{1 - f_{\tau_{\rm phys}}}$. The combinatorial

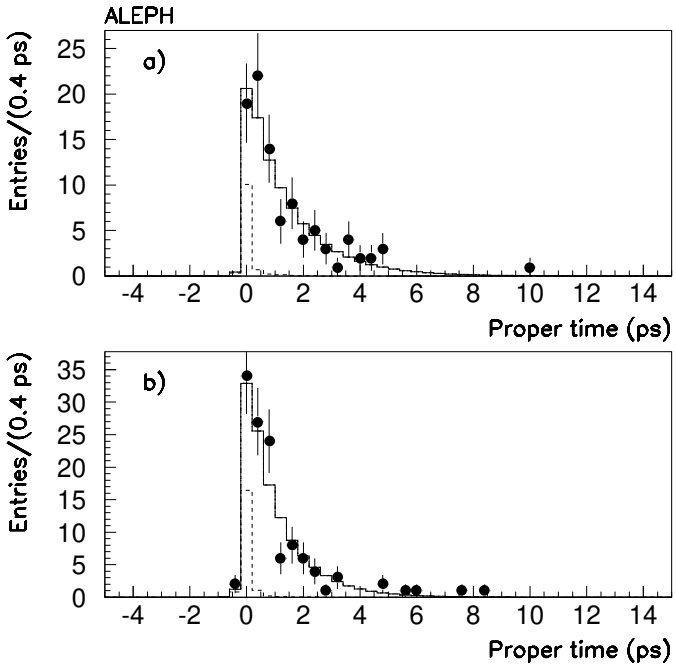

Figure 5: Proper time distributions for a) the B^- candidates, and b) the $\overline{B}^0$ candidates. The points represent the data, the solid line the result of the full fit and the dashed line the background component of the fit.

background proper time distribution $\mathcal{P}_{\rm comb}$ was a Gaussian centered at zero plus an exponential convolved with a Gaussian with a lifetime of $\tau_{\rm comb}$ and its fraction was $f_{\rm comb} = 1 - f_{\rm sig} - f_{\rm phys}$. Thus, there were only three free parameters in the fit: the two signal fractions $f^D_{\rm sig}$ and $f^\psi_{\rm sig}$, and the signal lifetime τ_B.

The fitted lifetime of the 94 B^- candidates is

$$\tau_- = 1.58^{+0.21}_{-0.18}\ {\rm ps},$$

with $f^D_{\rm sig} = 83.9^{+4.8}_{-5.5}\%$ and $f^\psi_{\rm sig} = 87.6^{+12.4}_{-20.7}\%$. For the 121 $\overline{B}^0$ candidates, the fitted lifetime is

$$\tau_0 = 1.25^{+0.15}_{-0.13}\ {\rm ps},$$

with $f^D_{\rm sig} = 78.0^{+5.1}_{-5.5}\%$ and $f^\psi_{\rm sig} = 93.5^{+6.5}_{-20.7}\%$. The proper time distributions together with the fit results are shown in Fig. 5. Fitting the two distributions simultaneously yields

$$\frac{\tau_-}{\tau_0} = 1.27^{+0.23}_{-0.19}.$$

4.4 Systematic uncertainties and checks

Systematic uncertainties from various sources were estimated and are summarized in Table 5.

It was mentioned in Sect. 4.2 that about 5% of the signal has a degraded boost resolution (corrupted signal) and taking this effect into account decreases slightly the

fitted lifetime by an amount taken as an asymmetric systematic uncertainty. Also, $f_{\tau_{\rm phys}}$ has been varied by $\pm 100\%$ (from 0 to 6.8% for the B^- sample and from 0 to 11.2% for the $\overline{B}^0$ sample) to estimate the systematic uncertainty from this physical background.

It was shown in Sect. 4.2 that there is a small contamination from other B hadrons in the signal samples. The effects of the contamination by $\overline{B}^0$ mesons in the B^- sample and by B^-, $\overline{B}^0_s$ and Λ^0_b hadrons in the $\overline{B}^0$ sample were estimated using the fitted B^- and $\overline{B}^0$ lifetimes and the $\overline{B}^0_s$ and Λ^0_b world average lifetimes [13] corrected by the use of the wrong mass when taken as $\overline{B}^0$ candidates.

The uncertainty on the background lifetime was estimated separately for the $B \to DX$ and $B \to \psi X$ channels by varying $f_{\tau_{\rm comb}}$ between the extreme values allowed from the fits to the background data. In the $B \to DX$ channels, the proper time distribution was also replaced by two Gaussians instead of one Gaussian plus an exponential.

The correction factor S has been varied between 1.0 and 1.5, the nominal value measured in the data being 1.27. Doubling the boost resolution does not change significantly the fit results.

Table 5: Systematic uncertainties on the fitted lifetimes from the fully reconstructed hadronic decays.

Source of uncertainty	τ_- (ps)	τ_0 (ps)	τ_-/τ_0
Corrupted signal and physical background	± 0.031	$^{+0.044}_{-0.042}$	$^{+0.020}_{-0.021}$
Contamination from other b hadrons	$^{+0.014}_{-0.000}$	$^{+0.001}_{-0.013}$	$^{+0.024}_{-0.002}$
$B \to DX$ background	$^{+0.014}_{-0.007}$	$^{+0.016}_{-0.010}$	$^{+0.002}_{-0.006}$
$B \to \psi X$ background	$^{+0.015}_{-0.011}$	± 0.001	$^{+0.010}_{-0.009}$
Correction factor S	$^{+0.001}_{-0.002}$	$^{+0.002}_{-0.001}$	$^{+0.001}_{-0.004}$
Total	$^{+0.040}_{-0.034}$	$^{+0.047}_{-0.045}$	$^{+0.033}_{-0.024}$

Any bias in the reconstructed proper time was excluded by obtaining the input lifetimes when fitting on a large sample of simulated signal events. The proper time distribution of the candidates selected from a simulated sample of 3.7 million $Z \to q\overline{q}$ events was also fitted taking into account the background. The result of this fit is also in agreement with the generated lifetime.

As a consistency check, the D meson lifetimes were also measured using the $B \to DX$ candidate events. The 29 $\overline{B}^0 \to D^+\pi^-$ candidates were used to measure the D^+ lifetime giving $\tau_{D^+} = 1.17^{+0.25}_{-0.19}$ ps, in agreement with the world average of $\tau_{D^+} = 1.057 \pm 0.015$ ps. The D^0 lifetime was also measured using the 154 $B^- \to D^0 X^-$ and $\overline{B}^0 \to D^{*+}(\to D^0\pi^+)X^-$ candidates. The result of the fit is $\tau_{D^0} = 0.407^{+0.038}_{-0.034}$ ps, in agreement with the world average of $\tau_{D^0} = 0.415 \pm 0.004$ ps [8].

5 Measurement using partially reconstructed hadronic $\overline{B}^0$ decays

To increase the reconstruction efficiency for the hadronic $\overline{B}^0$ decay modes

$$\begin{array}{rcl} \overline{B}^0 & \rightarrow & \pi_{\overline{B}}^- \quad X \quad D^{*+} \\ & & \qquad\quad \hookrightarrow \pi_D^+ D^0, \end{array} \tag{3}$$

$\overline{B}^0$ mesons were partially reconstructed by using the correlation between the $\pi_{\overline{B}}^-$ and π_D^+. The D^{*+} momentum can be approximated from the π_D^+ momentum alone with a precision of about 15% due to the small momentum transfer in the D^{*+} decay. This is not sufficient to distinguish between two body decays like $\overline{B}^0 \rightarrow \pi^- D^{*+}$ and $\overline{B}^0 \rightarrow \rho^- D^{*+}$ with a missing soft π^0 from the ρ^- decay. It does, however, allow an inclusive reconstruction of decays of the type (3) if the system X has low energy. The problem of approximating the $\overline{B}^0$ three-momentum from the $\pi_{\overline{B}}^-$ and π_D^+ momenta can be solved in the $\pi_{\overline{B}}^- \pi_D^+$ rest frame. Assuming a given XD^0 mass the $\overline{B}^0$ energy in this frame is

$$E_B^* = \frac{M_B^2 + M_{\pi_B \pi_D}^2 - M_{XD^0}^2}{2 M_{\pi_B \pi_D}}. \tag{4}$$

The XD^0 mass was set to $M_{XD^0} = 2.1$ GeV/c^2 to achieve the best momentum direction resolution (12 mrad in the laboratory frame) for a mixture of $\overline{B}^0 \rightarrow \pi^-(\rho^-) D^{*+}$ decays, the two decay modes for which the selection was optimized. For decays where the true missing mass is close to this value, the $\overline{B}^0$ flight direction in the $\pi_{\overline{B}}^- \pi_D^+$ rest frame is approximately the direction of the slow pion:

$$\vec{p}_B^{\,*} \approx \sqrt{(E_B^*)^2 - M_B^2} \cdot \frac{\vec{p}_{\pi_D}^{\,*}}{|\vec{p}_{\pi_D}^{\,*}|}. \tag{5}$$

The $\overline{B}^0$ momentum in the laboratory frame is obtained after a transformation from the $\pi_{\overline{B}}^- \pi_D^+$ rest frame to the laboratory frame. The momentum resolution is 2 GeV/c for $\overline{B}^0 \rightarrow \pi^-(\rho^-) D^{*+}$ decays and 8 GeV/c for the remaining decays contributing to the signal.

The calculation of the $\overline{B}^0$ momentum implicitly requires $M_{\pi\pi} < M_B - M_{XD^0} \approx 3.2$ GeV/c^2, while the kinematic limit for pions from reaction (3) is such that $M_{\pi_B \pi_D}$ is less than 1.5 GeV/c^2. Reconstructed $\overline{B}^0$ mesons are identified as an excess in the $\pi_{\overline{B}}^- \pi_D^+$ mass distribution below 1.5 GeV/c^2.

5.1 Candidate selection

Oppositely charged pion pairs $\pi_{\overline{B}}^- \pi_D^+$, consistent with coming from a common vertex within 3 standard deviations, were selected. The $\overline{B}^0$ momentum $\vec{p}_B$ was determined using the technique described above. Selecting events with high $\overline{B}^0$ momenta, 30 GeV/$c < |\vec{p}_B| <$ 45 GeV/c, and $\overline{B}^0$ decay angles such that $|\cos\theta^*_{B,\pi_{\overline{B}}^-}| < 0.8$ suppressed background and improved the determination of the $\overline{B}^0$ flight direction. Information from both the $\overline{B}^0$

production and decay vertices as well as the reconstructed jet direction were used to determine the quantity $\vec{\ell}_B$ (specifying both the $\overline{B}^0$ flight direction and decay length). The vector pointing from the primary vertex to the $\pi_B^- \pi_D^+$ vertex was combined with the jet direction using a χ^2 minimization. Jets were reconstructed with the JADE cluster algorithm [14] using $y_{cut} = 0.008$, which gives the best approximation of the $\overline{B}^0$ flight direction. The angular resolution obtained on $\vec{\ell}_B$ with this method is about 20 mrad. The $\overline{B}^0$ decay length $\vec{\ell}_B$ and the $\overline{B}^0$ momentum are independent measurements of the $\overline{B}^0$ flight direction. The angle between $\vec{\ell}_B$ and $\vec{p}_B$ was required to be less than 25 mrad. This cut decreases the efficiency slightly at small decay lengths, and this effect is taken into account in the lifetime fit.

Background candidates from $B^- \to \pi^- \pi^- X D^{*+}$ decays were identified and rejected. These candidates were selected by requiring an additional π^- coming from the secondary $\pi_B^- \pi_D^+$ vertex. The B^- momentum can be approximated from equation (5), replacing M_{XD^0} with M_{D^0} and the two-pion mass with the three-pion mass in formula (4). The angle between the B^- momentum and the flight direction was required to be smaller than 20 mrad. Excluding these events rejected 60% of $B^- \to \pi^- \pi^- X D^{*+}$ decays while only 20% of the $\overline{B}^0$ decays were lost.

The $\overline{B}^0$ lifetime was measured from candidates with a proper decay time

$$1 \text{ ps} < t = \frac{|\vec{\ell}_B| M_B}{|\vec{p}_B|} < 20 \text{ ps}.$$

At small decay lengths, background from light quark production is dominant. The resolution of the decay time is dominated by the uncertainty on the decay length. The resolution function, which enters in the lifetime fit, can be described by a sum of three Gaussians with widths of 260 μm, 780 μm and 4.9 mm, with relative fractions 0.71, 0.25 and 0.04, respectively. In this analysis, the distortion of the exponential decay distribution is mainly due to the third Gaussian since the cut on the decay time at 1 ps corresponds to a decay length of approximately 2 mm. The systematic uncertainty on the $\overline{B}^0$ lifetime was estimated by neglecting the third Gaussian (Table 7).

Fig. 6 shows the invariant $\pi_B^- \pi_D^+$ mass for the selected candidates. The lifetime was determined from candidates in the mass region 1 GeV/c^2 $< M_{\pi_B^- \pi_D^+} <$ 1.5 GeV/c^2. The sample consists of events where the π_D^+ and π_B^- originate from a $\overline{B} \to \pi_B^- X D^{*+} \to \pi_B^- X (\pi_D^+ D^0)_{D^{*+}}$ decay and of combinatorial background.

- $\overline{B}^0 \to \pi_B^- X (\pi_D^+ D^0)_{D^{*+}}$ signal events:
  The expected composition of the $\overline{B}^0 \to \pi_B^- X D^{*+} \to \pi_B^- X (\pi_D^+ D^0)_{D^{*+}}$ sample in the signal mass region 1 GeV/c^2 $< M_{\pi_B^- \pi_D^+} <$ 1.5 GeV/c^2 is given in Table 6. Branching ratios were taken from [15].

- $B^- \to \pi_B^- X (\pi_D^+ D^0)_{D^{*+}}$ background events:
  The amount of background from $B^- \to \pi_B^- X D^{*+}$ decays was estimated from a Monte Carlo simulation to be $r_- \equiv B^-/(B^- + \overline{B}^0) = (8.3 \pm 2.4)\%$ (Table 6). $B^- \to \pi^-, \rho^- D^{**0}$ decays were simulated with relative rates according to [16] and normalized to the measured $B^- \to \pi^- \pi^- D^{*+}$ branching ratio [15]. The ratio r_- can be determined as well from the number of rejected B^- candidates ($r_- = 3.2 \pm 5.6\%$). For the lifetime fit the ratio from the Monte Carlo simulation

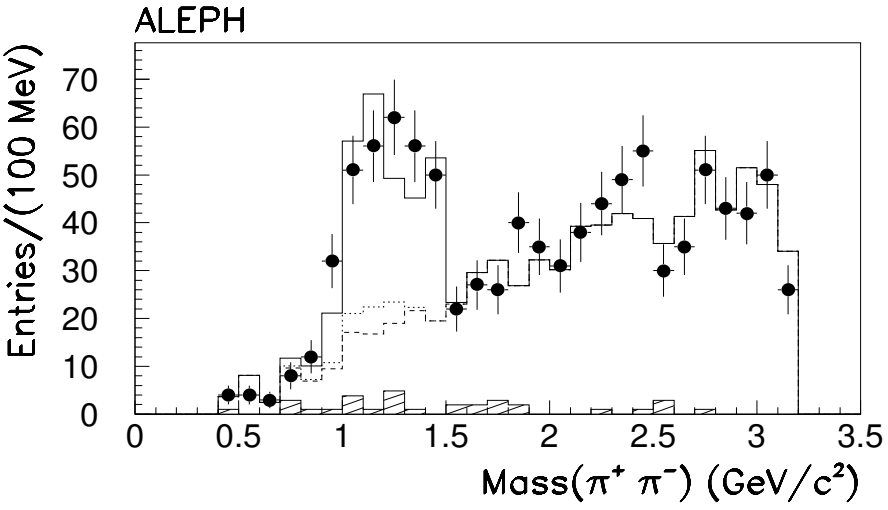

Figure 6: $\pi_B^- \pi_D^+$ mass distributions. Shown are the data (with error bars) and the Monte Carlo simulation (histograms). The contributions from light quark background (hatched), $b\bar{b}$ background (dashed), $B^- \to \pi_B^- X D^{*+}$ (dotted) and the $\overline{B}^0 \to \pi_B^- X D^{*+}$ signal (full) are added.

was taken with a systematic uncertainty given by the difference of the two estimates: $r_- = (8.3 \pm 2.4 \pm 5.1)\%$.

- Combinatorial background:
  The shape of the combinatorial background was estimated from a Monte Carlo simulation. Fig. 6 shows the $\pi_B^- \pi_D^+$ mass spectrum for this background in Monte Carlo events. The background spectrum was normalized to the data in the region $M_{\pi\pi} > 1.5$ GeV/c^2, where $B \to \pi_B^- X D^{*+} \to \pi_B^- X \pi_D^+ D^0$ events cannot contribute. The number of background events $N_b = 94.0 \pm 9.6$ was obtained from an extrapolation to the signal mass region, 1 GeV/$c^2 < M_{\pi_B^- \pi_D^+} < 1.5$ GeV/c^2.

A background sample, consisting of three subsamples, was selected from data to describe the combinatorial background time distribution. The first subsample was selected from wrong charge combinations $\pi_B^\pm \pi_D^\pm$ applying the same selection criteria as for the signal sample. The fact that slow pions are distributed isotropically around the jet axis motivates the selection of the second subsample with opposite signed pions. The momentum of the slow pion was first rotated around the jet axis $\vec{p}_{\pi_D} \to \vec{p}\,'_{\pi_D}$ so that the momentum difference $|\vec{p}_{\pi_D} - \vec{p}\,'_{\pi_D}|$ is 200 MeV/c with a maximal rotation angle of $\pm 90°$. Then the normal selection was applied. Real $B \to \pi_B^- X (\pi_D^+ D^0)_{D^{*+}}$ decays do not pass the cut on the angle between $\vec{\ell}_B$ and $\vec{p}_B$ since the $\vec{p}_{\pi_D}$ rotation changes the reconstructed B momentum. The third subsample consists of wrong sign combinations with a rotation of the slow pion.

Table 6: Expected number of events in the signal mass region, 1 GeV/c^2 < $M_{\pi_B^- \pi_D^+}$ < 1.5 GeV/c^2. A total of 275 events were observed in the data.

		events expected	
$\overline{B}^0 \rightarrow$	$\pi^-\ D^{*+}$	57.3	
	$\rho^-\ D^{*+}$	44.5	
	$\pi^-\ D^{**}$, $\rho^-\ D^{**}$	7.2	
	other two body decays with a D^{*+}	3.2	
	$(\pi^-\ \pi^0)_{\text{non-resonant}}\ D^{*+}$	18.9	163 ± 17
	$(\pi\ \rho)_{\text{non-resonant}}\ D^{*+}$	6.3	
	$e^-\ \overline{\nu}\ D^{*+}$, $\mu^-\ \overline{\nu}\ D^{*+}$	9.5	
	other three body decays with a D^{*+}	13.3	
	four body decays with a D^{*+}	3.1	
$B^- \rightarrow$	$\pi^-\ D^{**}$	10.2	
	$\rho^-\ D^{**}$	2.2	$14.7^{+3.9}_{-4.0}$
	other decays with a D^{*+}	2.3	
$b\bar{b}$ background			83.4 ± 9.2
$q\overline{q}$ background			10.6 ± 3.3
Sum			272 ± 20

5.2 $\overline{B}^0$ lifetime measurement

The lifetime was determined with a simultaneous unbinned maximum likelihood fit to the signal and background samples. Six events included in the analysis with fully reconstructed $\overline{B}^0$ decays and one event reconstructed as a semileptonic $\overline{B}^0$ decay were rejected. The likelihood function, which depends on eight fit parameters (τ_0, N_s, N_-, N_b, τ_-^{eff}, r_b, τ_{b1}, τ_{b2}), can be written

$$
\begin{aligned}
\mathcal{L} \;=\; & \exp\!\left(-\frac{1}{2}(N_b - \langle N_b\rangle)^2/\sigma^2_{N_b}\right)\exp\!\left(-\frac{1}{2}(r_- - \langle r_-\rangle)^2/\sigma^2_{r_-}\right) \\
\times\; & \exp\!\left(-\frac{1}{2}(\tau_- - \langle \tau_-\rangle)^2/\sigma^2_{\tau_-}\right)\exp(-N_s - N_- - N_b) \\
\times\; & \prod_i^{\text{signal sample}} \left[N_s\mathcal{P}_s(t_i;\tau_0) + N_-\mathcal{P}_-(t_i;\tau_-^{\text{eff}}) + N_b\mathcal{P}_b(t_i;r_b,\tau_{b1},\tau_{b2})\right] \\
\times\; & \prod_i^{\text{backg. sample}} \mathcal{P}_b(t_i;r_b,\tau_{b1},\tau_{b2}),
\end{aligned}
$$

where N_s, N_- and N_b are the number of signal events, the number of $B^- \rightarrow \pi_{\overline{B}} X D^{*+}$ background events and the amount of combinatorial background, respectively.

The time distribution for the $\overline{B}^0$ signal events $\mathcal{P}_s$ is an exponential folded with the momentum and decay length resolution functions, taking into account the momentum and decay length dependent reconstruction efficiency and the momentum distribution. The resolution functions, efficiency and momentum distribution were taken from simulated events.

A normalized exponential with an effective lifetime $\tau_-^{\rm eff}$ was taken for the $B^- \to \pi_B^- X D^{*+}$ background time distribution $\mathcal{P}_-(t, \tau_-^{\rm eff})$.

The time distribution $\mathcal{P}_b$ for the combinatorial background was described by the sum of two normalized exponentials with lifetimes τ_{b1} and τ_{b2} with relative contributions of r_b and $(1 - r_b)$.

Three constraints are included in the likelihood function. The amount of combinatorial background N_b was determined from the $\pi_B^- \pi_D^+$ mass spectrum to be $\langle N_b \rangle = 94.0 \pm 9.6$. The ratio $r_- = N_-/(N_s + N_-)$ of $B^- \to \pi_B^- X D^{*+}$ to $B \to \pi_B^- X D^{*+}$ events in the signal sample was estimated to be $\langle r_- \rangle = 8.3 \pm 5.6\%$. The effective B^- lifetime of $\langle \tau_-^{\rm eff} \rangle = 1.04 \pm 0.17$ ps was obtained from a simulation using the world average B^- lifetime $\tau_- = 1.617 \pm 0.046$ ps [13]. The uncertainty on $\tau_-^{\rm eff}$ is the statistical uncertainty from the simulation. The bias to a smaller effective B^- lifetime is due to the rejection of B^- decays, identified with an additional pion, which is more efficient for long decay lengths.

Fig. 7 shows the proper time spectrum for the signal and background samples together with the fit result. The lifetime was determined to be

$$\tau_0 = 1.49 \; ^{+0.17}_{-0.15}({\rm stat})^{+0.08}_{-0.06}({\rm syst}) \text{ ps}.$$

The sources of systematic uncertainties are given in Table 7. The largest contribution comes from the uncertainty on the background time distribution. The assumption that the background sample describes the real background in the signal sample has been checked with Monte Carlo events and was found to be valid within the statistical uncertainties. The corresponding systematic uncertainty is the statistical uncertainty from the Monte Carlo simulation.

Table 7: Systematic uncertainties on the fitted lifetime from the partially reconstructed hadronic $\overline{B}^0$ decays.

Source of uncertainty	τ_0 (ps)
Background time distribution	$^{+0.057}_{-0.044}$
Efficiency (MC statistics)	$^{+0.037}_{-0.020}$
Efficiency (parametrization, signal composition)	± 0.019
Momentum and decay length resolution	± 0.024
Parametrization of $\mathcal{P}_-(t)$ and $\mathcal{P}_b(t)$	± 0.011
Fragmentation function ($\epsilon_b = 0.0032 \pm 0.0017$) [17]	$^{+0.006}_{-0.008}$
B^- lifetime ($\tau_{B^-} = 1.617 \pm 0.046$ ps)	∓ 0.002
Total	$^{+0.076}_{-0.059}$

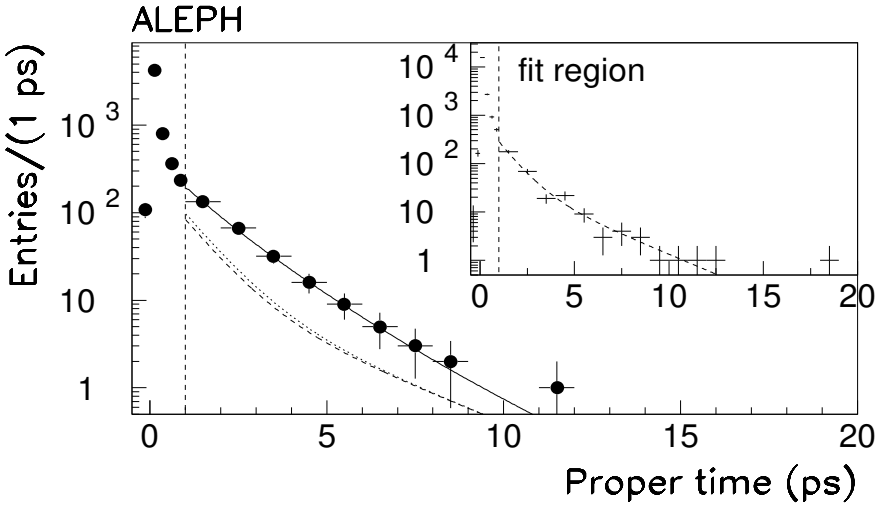

Figure 7: Fit results for the signal and the background sample (inset). For the signal sample the dashed and dotted curves are the combinatorial background contribution and the total background, including $B^- \to \pi^- X D^{*+}$ decays, respectively.

6 Conclusions

The lifetimes of the $\overline{B}^0$ and B^- mesons have been measured with the ALEPH detector at LEP, using three different methods. The method using $D^{(*)}\ell$ correlations yielded

$$\begin{aligned} \tau_0 &= 1.61 \pm 0.07 \pm 0.04 \text{ ps}, \\ \tau_- &= 1.58 \pm 0.09 \pm 0.04 \text{ ps}, \\ \frac{\tau_-}{\tau_0} &= 0.98 \pm 0.08 \pm 0.03. \end{aligned}$$

A second method, using fully reconstructed hadronic $\overline{B}^0$ and B^- decays, obtained

$$\begin{aligned} \tau_0 &= 1.25^{+0.15}_{-0.13} \pm 0.05 \text{ ps}, \\ \tau_- &= 1.58^{+0.21+0.04}_{-0.18-0.03} \text{ ps}, \\ \frac{\tau_-}{\tau_0} &= 1.27^{+0.23+0.03}_{-0.19-0.02}. \end{aligned}$$

Finally, a method that uses a partial reconstruction technique to identify $\overline{B}^0 \to D^{*+}\pi^- X$ decays gave the result

$$\tau_0 = 1.49^{+0.17+0.08}_{-0.15-0.06} \text{ ps}.$$

Events that were selected by more than one analysis were retained only once, such that the three measurements are statistically independent. A total of eight events were removed in this way. Combined results were obtained by summing the log-likelihood functions of the analyses. In this way the means and statistical uncertainties were obtained. The different nature of the analyses leads to independent systematic uncertainties, permitting the use of a simple weighted average for the combined systematic uncertainties.

The combined results, which supersede previous ALEPH measurements of the $\overline{B}^0$ and B^- lifetimes [2], are

$$\begin{aligned} \tau_0 &= 1.55 \pm 0.06 \pm 0.03 \text{ ps}, \\ \tau_- &= 1.58 \pm 0.09 \pm 0.03 \text{ ps}, \\ \frac{\tau_-}{\tau_0} &= 1.03 \pm 0.08 \pm 0.02. \end{aligned}$$

These combined results represent the most precise measurements to date of the $\overline{B}^0$ and B^- lifetimes and their ratio [2, 3]. They are consistent with theoretical expectations; however, the current precision of the measurements does not yet probe lifetime differences below the 5% level, which is the region of theoretical interest. The current precision is sufficient for other purposes, for example in the extraction of $|V_{cb}|$ using the decay $\overline{B}^0 \to D^{*+}\ell^-\overline{\nu}_\ell$ [18, 19].

7 Appendix - Determination of sample compositions for the $D^{(*)}\ell$ analysis

Table 8 shows the six $\overline{B}^0$ decay channels considered in the determination of the sample composition coefficients. Possible modes with two or more non-resonant pions in the final state or with D^{**} decaying into $D^{(*)}$ plus two or more pions were assumed negligible. The branching ratios of the modes considered have been determined in the following way:

1. B_1 and B_2 have been taken from measurements at CLEO and ARGUS [8, 19, 20, 21].

2. It was assumed that the inclusive semileptonic branching ratio of $\overline{B}^0$ mesons is given by the sum of the exclusive channels considered,

$$B_\ell \equiv B(\overline{B}^0 \to \ell^- X) = \sum_{i=1}^{6} B_i.$$

   This quantity has also been measured at CLEO and ARGUS [22].

3. The ALEPH measurement [23] of

$$B(b \to D^{*+}\pi^-\ell^-\nu X) = (3.6 \pm 1.2) \times 10^{-3}$$

   has been used to determine B_4^-. It has been assumed that this final state comes from B^- decays. Thus, dividing by the fraction of b quarks hadronizing into B^- ($f_d = 0.388 \pm 0.025$ [18, 24]) one obtains

$$B_4^- = B(B^- \to D^{*+}\pi^-\ell^-\nu) = (9.3 \pm 3.2) \times 10^{-3}.$$

4. In decays of the type $\overline{B} \to D^{(*)}\pi\ell\nu$, it was assumed that the $D^{(*)}\pi$ states are produced with a fixed value of isospin, $I = 1/2$ (as is the case if the decay proceeds via D^{**}). Then isospin conservation implies

$$n \equiv \frac{B_4}{B_3} = \frac{B_6}{B_5} = 2.$$

Table 8: $\overline{B}^0$ semileptonic branching ratios for $\tau_0 = \tau_-$. The corresponding B^- decay channels are also listed. The uncertainties on B_3–B_6 are large and highly correlated and are therefore not shown. Quantities with uncertainties shown are independent.

$\overline{B}^0$ BR (%)		Corresponding B^- Decay
$B_1 = B(\overline{B}^0 \to D^{*+}\ell^-\nu)$	$= 4.50 \pm 0.45$	$B_1^- = B(B^- \to D^{*0}\ell^-\nu)$
$B_2 = B(\overline{B}^0 \to D^{+}\ell^-\nu)$	$= 1.9 \pm 0.5$	$B_2^- = B(B^- \to D^{0}\ell^-\nu)$
$B_3 = B(\overline{B}^0 \to D^{*+}\pi^0\ell^-\nu)$	$= 0.49$	$B_3^- = B(B^- \to D^{*0}\pi^0\ell^-\nu)$
$B_4 = B(\overline{B}^0 \to D^{*0}\pi^+\ell^-\nu)$	$= 0.93$	$B_4^- = B(B^- \to D^{*+}\pi^-\ell^-\nu) = 0.93 \pm 0.32$
$B_5 = B(\overline{B}^0 \to D^{+}\pi^0\ell^-\nu)$	$= 0.95$	$B_5^- = B(B^- \to D^{0}\pi^0\ell^-\nu)$
$B_6 = B(\overline{B}^0 \to D^{0}\pi^+\ell^-\nu)$	$= 1.90$	$B_6^- = B(B^- \to D^{+}\pi^-\ell^-\nu)$
$B_\ell = B(\overline{B}^0 \to \ell X)$	$= 10.4 \pm 1.1$	

Table 9: Contributions of $\overline{B}^0$ and B^- decays to the $D^{*+}\ell^-$ and $D^0\ell^-$ event samples.

	$D^{*+}\ell^-$	$D^0\ell^-$
$\overline{B}^0$	$B_* B_1 + \epsilon_+^{**} B_* B_3$	$\epsilon_{\delta m}(B_* B_1 + \epsilon_0^{**} B_* B_3) + \epsilon_0^{**}(B_4 + B_6)$
B^-	$\frac{\tau_-}{\tau_0}\left[\epsilon_+^{**} B_* B_4\right]$	$\frac{\tau_-}{\tau_0}\left[B_1 + B_2 + \epsilon_0^{**}(B_3 + B_5) + \epsilon_0^{**}\epsilon_{\delta m} B_* B_4)\right]$

These conditions along with Eq. 2 permit the calculation of all the necessary $\overline{B}^0$ and B^- branching ratios. The uncertainties on these branching ratios are large and highly correlated and thus not very meaningful. The quantities B_ℓ, B_1, B_2 and B_4^- are the independent quantities used to calculate the $\overline{B}^0$ semileptonic branching fractions. They have been varied independently for the evaluation of the systematic uncertainty on the fitted lifetimes.

The contributions to the $D^{*+}\ell^-$ and $D^0\ell^-$ samples were calculated using these branching ratios, the branching ratio for $D^{*+} \to D^0\pi^+$ ($B_* = 0.68 \pm 0.03$ [8]), and the relative efficiency for detecting channels B_3–B_6 ($\epsilon_+^{**} = 0.75 \pm 0.10$ for $D^{*+}\ell^-$ and $\epsilon_0^{**} = 0.62 \pm 0.10$ for $D^0\ell^-$, determined using a Monte Carlo simulation). The probability that a $D^{*+}\ell^-$ event is mistakenly reconstructed as a $D^0\ell^-$ event ($\epsilon_{\delta m} = 0.16 \pm 0.03$) was also taken into account. Table 9 shows the $\overline{B}^0$ and B^- contributions to the $D^{*+}\ell^-$ and $D^0\ell^-$ samples.

Acknowledgments

We thank our colleagues in the accelerator divisions for the continued good performance of LEP. Thanks also to the many engineering and technical personnel at CERN and at the home institutes for their contributions to the performance of the ALEPH detector. Those of us from non-member states thank CERN for its hospitality.

References

[1] I. Bigi *et al.*, "Non-leptonic Decays of Beauty Hadrons - From Phenomenology to Theory," (CERN-TH.7132/94) from the second edition of the book "B Decays", S. Stone (ed.) World Scientific.

[2] D. Buskulic *et al.*, (ALEPH Collaboration), Phys. Lett. **B307** (1993) 194.

[3] P. Abreu *et al.*, (DELPHI Collaboration), Z. Phys. **C68** (1995) 13;
P. Abreu *et al.*, (DELPHI Collaboration), "Lifetimes of Charged and Neutral B Hadrons Using Event Topology," CERN-PPE/95-59, submitted to Z. Phys. C;
R. Akers *et al.*, (OPAL Collaboration), Z. Phys. **C67** (1995) 379;
F. Abe *et al.*, (CDF Collaboration), Phys. Rev. Lett. **72** (1994) 3456.

[4] D. Decamp *et al.*, (ALEPH Collaboration), Nuc. Instr. Meth. **A294** (1990) 121.

[5] G. Batignani *et al.*, "Recent Results and Running Experience of the New ALEPH Vertex Detector", Conference Record of the 1991 IEEE Nuclear Science Symposium, November 2-9, 1991, Santa Fe, New Mexico, USA.

[6] D. Buskulic *et al.*, (ALEPH Collaboration), Nucl. Instr. Meth. **A360** (1995) 481.

[7] D. Buskulic *et al.*, (ALEPH Collaboration), Nucl. Instr. Meth. **A346** (1994) 461.

[8] Particle Data Group, Phys. Rev. **D50** (1994) 1173.

[9] D. Buskulic *et al.*, (ALEPH Collaboration), Phys. Lett. **B313** (1993) 535.

[10] D. Buskulic *et al.*, (ALEPH Collaboration), Phys. Lett. **B357** (1995) 699.

[11] D. Bortoletto *et al.*, (CLEO Collaboration), Phys. Rev. Lett. **64** (1990) 2117;
H. Albrecht *et al.*, (ARGUS Collaboration), Z. Phys. **C54** (1992) 1.

[12] D. Buskulic *et al.*, (ALEPH Collaboration), Phys. Lett. **B343** (1995) 444;
M. Acciarri *et al.*, (L3 Collaboration), Phys. Lett. **B332** (1995) 201.

[13] H.-G. Moser, "LEP B-Lifetimes", to be published in the proceedings of the International Europhysics Conference on High Energy Physics, July/August 1995, Brussels, Belgium.

[14] S. Bethke *et al.*, (JADE Collaboration), Phys. Lett. **B213** (1988) 235.

[15] M.S. Alam *et al.*, (CLEO Collaboration), Phys. Rev. **D50** (1994) 43;
C. Bebek *et al.*, (CLEO Collaboration), Phys. Rev. **D36** (1987) 1289;
A.Albrecht *et al.*, (ARGUS Collaboration), Z. Phys. **C48** (1990) 543;
D. Bortoletto *et al.*, (CLEO Collaboration), Phys. Rev. **D45** (1992) 21.

[16] P. Colangelo, F. De Fazio, G. Nardulli, Phys. Lett. **B303** (1993) 152. a_1 and a_2 were set to 1.15 and 0.26, respectively.

[17] D. Buskulic *et al.*, (ALEPH Collaboration), Z. Phys. **C62** (1994) 179.

[18] D. Buskulic *et al.*, (ALEPH Collaboration), Phys. Lett. **B359** (1995) 236.

[19] B. Barish *et al.*, (CLEO Collaboration), Phys. Rev. **D51** (1995) 1014.

[20] H. Albrecht *et al.*, (ARGUS Collaboration), Phys. Lett. **B324** (1994) 249.

[21] H. Albrecht *et al.*, (ARGUS Collaboration), Z. Phys. **C57** (1993) 533.

[22] M. Athanas *et al.*, (CLEO Collaboration), Phys. Rev. Lett. **73** (1994) 3503.

[23] D. Buskulic *et al.*, (ALEPH Collaboration), Phys. Lett. **B345** (1994) 103.

[24] D. Buskulic *et al.*, (ALEPH Collaboration), Phys. Lett. **B361** (1995) 221.